

U.S. DEPARTMENT OF COMMERCE
National Oceanic and Atmospheric Administration
Environmental Research Laboratories

NOAA Technical Memorandum ERL NSSL-57

NUMERICAL SIMULATION
OF CONVECTIVE VORTICES

Robert P. Davies-Jones
National Severe Storms Laboratory, NOAA
Norman, Oklahoma

Glenn T. Vickers
Advanced Study Program
National Center for Atmospheric Research
Boulder, Colorado

Property of
NWC Library
University of Oklahoma

National Severe Storms Laboratory
Norman, Oklahoma
November 1971



TABLE OF CONTENTS

	<u>Page</u>
ABSTRACT	v
1. INTRODUCTION	1
2. MATHEMATICAL FORMULATION	3
3. LINEARIZED SOLUTIONS	6
4. NUMERICAL METHOD	8
5. RESULTS	11
5.1 Selection of Flow Parameters	11
5.2 Test of Stretched Coordinate System	12
5.3 Case with Rigid Bottom Surface ($K=0$)	13
5.4 Case with Free Bottom Surface	19
5.5 Effects of Varying Flow Parameters	23
6. CONCLUSIONS	24
7. ACKNOWLEDGMENTS	25
8. REFERENCES	26

NUMERICAL SIMULATION OF CONVECTIVE VORTICES

Robert P. Davies-Jones
National Severe Storms Laboratory, NOAA
Norman, Oklahoma

and

Glenn T. Vickers¹
Advanced Study Program
National Center for Atmospheric Research²
Boulder, Colorado

ABSTRACT

We present a numerical model of axisymmetric thermal convection with swirl in a non-rotating cylinder with height-to-radius of order unity. The top and bottom are kept at uniform temperatures, and the rim is assumed to be a perfect insulator. In general, the top and the rim are free boundaries, while at the bottom we apply either no-slip, no-stress, or the turbulent conditions used by Kuo (1971). Initially, the fluid is unstably stratified and swirling, and the subsequent flow is determined by numerically solving the initial value problem. The model is crudely applicable to dust-devils although the top and side and the use of constant eddy diffusivities are unrealistic features.

We show how Arakawa's conservative scheme for the Jacobian can be generalized to an irregular mesh. We are thus able to improve the resolution in the boundary layers without increasing the number of grid points.

Within certain ranges of the flow parameters, the flow consists of a one-cell meridional circulation, and forms a transient concentrated vortex near the axis. With a non-slip bottom, the vortices are comparable in angular velocity amplification (~ 30 times initial value) with those obtained by Leslie (1971), using a similar model but with externally supplied buoyancy. With a free bottom, we get amplifications of up to 300 times.

-
- 1 On leave from the Department of Applied Mathematics and Computing Science, The University of Sheffield, England.
 - 2 The National Center for Atmospheric Science is sponsored by the National Science Foundation.

NUMERICAL SIMULATION OF CONVECTIVE VORTICES

Robert P. Davies-Jones and Glenn T. Vickers

1. INTRODUCTION

Concentrated vortices have been generated successfully in the laboratory by a number of investigators. The rotation introduced into the system by rotating a tank of water (Long, 1956, 1958; Turner and Lilly, 1963; Turner, 1966) or an outer screen if air is the working fluid (Barcilon, 1967; Ying and Chang, 1970; Ward, 1970) is concentrated into a vortex by establishing meridional circulations in the fluid. The driving mechanism is provided by extracting fluid from the top or bottom of the apparatus (Long, Ying and Chang, Ward), by the drag of rising gas bubbles released near the axis of the tank (Turner and Lilly, Turner), or by heating the bottom plate (Barcilon). Although all maintain constant rotation to achieve a steady state, Ward (private communication) has demonstrated that a transient vortex is formed when the screen, initially at rest, is given a small impulse.

Theoretical vortex models, on the other hand, have not been nearly as successful. The steady state similarity solutions, generated by Burgers (1948), Gutman (1957), Sullivan (1959), Kuo (1966) and many others, while ingenious, suffer from important drawbacks, notably non-satisfaction of boundary conditions both at the ground where slip occurs (with the exception of Serrin's (1971) solution) and at infinity where the vertical velocity is generally infinite. However, Turner (1966) has been quite successful in approximately matching a boundary layer solution to an interior solution. By assuming that pressure deviation from a basic state is a function of radius only, solutions such as Kuo's (1966) also fail in the zero order to represent the inhibiting effect that the centrifugal force has on the convective meridional circulations. Similarity solutions are also unable to describe the time evolution of a vortex during its developing stages. Only Gutman (1957) and Kuo (1966) include thermodynamic buoyancy forces and attempt to model atmospheric vortices. Kuo obtains both one and two-cell solutions, but the downdraft in his two-cell vortex is cold (not likely for reasons pointed out by Lilly, 1969).

With the advent of fast computers it is now possible to attempt numerically the time dependent problem of vortex formation, starting from suitable initial conditions. There have been various previous investigations. Inman (1966) has generalized Ogura's (1963) numerical study of a moist convective element released in a shallow, conditionally unstable atmosphere by introducing rotation. Unfortunately, he was not able to integrate long enough to reach a steady state, his numerical scheme was neither energy nor vorticity conserving, and the boundary conditions were not realistic as the bottom is free while on the side zonal velocity is fixed but the vertical shear stress vanishes (i.e., the side is neither free nor rigid). Work on this model has been continued by Wilkins,

Sasaki and Schauss (1971). If we define a swirl amplification factor, S , as the ratio of the maximum swirl velocity ever attained to the maximum swirl velocity present initially, and r_{\max} as the radius at which this maximum swirl velocity is reached, then in their model S is less than two (although it is presumably still increasing at termination) and r_{\max} is typically one-tenth of the radius of the system. The convective cells in the atmosphere which form tornadoes and dust-devils probably are much more efficient at concentrating vorticity.

Leslie (1971) has numerically simulated the carbonated water vortex experiments of Turner and Lilly (1963) and Turner (1966) [but at higher Rossby number]. He used the conservative numerical schemes devised by Arakawa (1966) and integrated to a steady state. He obtained values of S of 2.2 for a free top and 2.9 for a rigid top, with r_{\max} approximately equal to one-tenth of the tank radius. His work is not directly applicable to the atmosphere because the fluid is in a rotating tank, and because he was forced to maintain an artificially prescribed buoyancy force in the neighborhood of the axis to simulate the drag of rising gas bubbles.

In addition, Wippermann, Berkofsky and Szillinsky (1969) have investigated numerically the formation of a tornado funnel under an intensifying vortex. However, as pointed out by Leslie, Morton and Smith (1970), the development of the funnel was greatly speeded up by an artificial generation of vorticity created by their numerical scheme. It therefore seems vital to use a conservative scheme.

In our work we model Kuo's idea (1966) that pre-existing ambient vorticity is drawn inward and concentrated by thermal convection. Our work differs from Leslie's in that the buoyancy force, driving the meridional circulations, is thermal in origin and is maintained by keeping a constant temperature difference between the top and bottom plates of a cylinder containing air. We thus have an extra equation, describing the thermodynamics of the system, to lift the restriction of a prescribed buoyancy force. Note that the formation of a strong vortex may be hindered here by the breakdown of the meridional circulation into two or more cells. These two cell solutions are undesirable: they do not resemble a two cell vortex since the inner cell is comparable in size with the outer cell, and the vortex that eventually forms is contained in the downdraft of the inner cell. In addition, the outer rim is not generally rotated so that angular momentum is supplied only through initial swirl, and the vortex that forms is transient rather than steady.

Our model applies very crudely to the formation of (stationary) dust devils although it contains many features not found in the atmosphere such as an artificial isothermal lid, an isothermal ground, artificial side boundary to close the system, constant eddy diffusivity, and inadequate resolution of the thin thermal boundary layer which exists next to the ground under dust-devil conditions (Ryan and Carroll, 1970).

2. MATHEMATICAL FORMULATION

Ogura and Phillips (1962) showed that over depths of 3 km or less in the atmosphere the Boussinesq approximation is valid. After making this approximation, introducing terms for the turbulent eddy mixing of momentum and heat, and assuming axisymmetry, their 'anelastic' equations become (in cylindrical coordinates)

$$\frac{\partial u}{\partial t} + u \frac{\partial u}{\partial r} + w \frac{\partial u}{\partial z} - \frac{v^2}{r} = -c_p \theta \frac{\partial \pi'}{\partial r} + \nu \left(\nabla^2 u - \frac{u}{r^2} \right) \quad (1)$$

$$\frac{\partial v}{\partial t} + u \frac{\partial v}{\partial r} + w \frac{\partial v}{\partial z} + \frac{uv}{r} = \nu \left(\nabla^2 v - \frac{v}{r^2} \right) \quad (2)$$

$$\frac{\partial w}{\partial t} + u \frac{\partial w}{\partial r} + w \frac{\partial w}{\partial z} = -c_p \theta \frac{\partial \pi'}{\partial z} + \frac{g\varphi'}{\theta} + \nu \nabla^2 w \quad (3)$$

$$\frac{\partial \varphi'}{\partial t} + u \frac{\partial \varphi'}{\partial r} + w \frac{\partial \varphi'}{\partial z} = \kappa \nabla^2 \varphi' \quad (4)$$

$$\frac{\partial(ru)}{\partial r} + \frac{\partial(rw)}{\partial z} = 0 \quad (5)$$

where u , v , w are the velocities in the r , ϕ and z directions, c_p is the specific heat at constant pressure, φ' is the deviation of potential temperature from that in a dry adiabatic atmosphere of constant potential temperature θ , g is acceleration due to gravity, ν and κ are the eddy viscosity and thermal diffusivity which are assumed to be equal constants, and π' is the deviation of $\pi [\equiv (p/P)^{R/c_p}]$ where R is the gas constant for dry air, p is pressure and P is a constant reference pressure (1000 mb)] from that in the dry adiabatic reference atmosphere. Note that, after Leslie (1971), we assume that we can neglect variations of density in the centrifugal force, and deformation of the free top.

We assume that the air is bounded vertically by an isothermal ground ($z = 0$) and a free layer at $z = H$ which is maintained at temperature θ . To obtain a closed system we place a side boundary at $r = L$, the effect of which is minimized by assuming that it is free and insulating so that only the normal component of velocity vanishes there. L/H defines the aspect ratio of the cylindrical flow region. At the ground we adopt the turbulent

boundary conditions on velocity used by Kuo (1971), applicable at the top of the laminar sub-layer. In summary, the boundary conditions are

$$u - K \frac{\partial u}{\partial z} = v - K \frac{\partial v}{\partial z} = w = 0, \quad \varphi' = \gamma H \quad \text{at } z = 0$$

$$\frac{\partial u}{\partial z} = \frac{\partial v}{\partial z} = w = \varphi' = 0 \quad \text{at } z = H$$

$$u = \frac{\partial}{\partial r} \left(\frac{v}{r} \right) = \frac{\partial w}{\partial r} = \frac{\partial \varphi'}{\partial r} = 0 \quad \text{at } r = L$$

where K is a constant ($= 0$ for no-slip, $= \infty$ for free boundary) and γ is the mean potential temperature lapse rate between $z = 0$ and H . Note that if an identical turbulent boundary condition on temperature had also been chosen, the limit $K = \infty$ would not have any interest since the ground would then act as a perfect insulator. Other boundary conditions were also tried, and are described later. In addition, we require that

$$u = v = \frac{\partial w}{\partial r} = \frac{\partial \varphi'}{\partial r} = 0 \quad \text{at } r = 0 \text{ (axis)}.$$

We define non-dimensional variables (denoted by the subscript*) as follows:

$$(r_*, z_*) \equiv H^{-1}(r, z)$$

$$(u_*, v_*, w_*) \equiv R_a^{-1} H K^{-1}(u, v, w)$$

$$\varphi'_* = (\gamma H)^{-1} \varphi'$$

$$t_* = \kappa H^{-2} t$$

where R_a is defined below. [We discovered later that $R_a^{\frac{1}{2}} H^{-1} \kappa$ would have been a better choice for characteristic velocity.]^a Henceforth, we shall drop the subscripts and assume that these variables are non-dimensional unless otherwise stated.

If, in addition, we introduce the Stokes's streamfunction, ψ , given by $u = \frac{1}{r} \frac{\partial \psi}{\partial z}$, $w = -\frac{1}{r} \frac{\partial \psi}{\partial r}$, and form the equation for η , the ϕ component of vorticity ($\equiv \frac{\partial u}{\partial z} - \frac{\partial w}{\partial r}$), we obtain the following set of equations

$$\frac{\partial \eta}{\partial t} = R_a \left[J_{rz} \left(\frac{\eta}{r}, \psi \right) + \frac{1}{r} \frac{\partial v^2}{\partial z} \right] + \sigma \left[\nabla^2 \eta - \frac{\eta}{r^2} - \frac{\partial \varphi'}{\partial r} \right] \quad (6)$$

$$\frac{\partial v}{\partial t} = \frac{R_a}{r^2} J_{rz} (vr, \psi) + \sigma \left[\nabla^2 v - \frac{v}{r^2} \right] \quad (7)$$

$$\frac{\partial \varphi'}{\partial t} = \frac{R_a}{r} J_{rz} (\varphi', \psi) + \nabla^2 \varphi' \quad (8)$$

$$\eta = \frac{1}{r} \frac{\partial^2 \psi}{\partial z^2} + \frac{1}{r} \frac{\partial^2 \psi}{\partial r^2} - \frac{1}{r^2} \frac{\partial \psi}{\partial r} \quad (9)$$

where J_{rz} , the Jacobian operator, is defined by

$$J_{rz} (p, q) \equiv \frac{\partial p}{\partial z} \frac{\partial q}{\partial r} - \frac{\partial p}{\partial r} \frac{\partial q}{\partial z},$$

$R_a \equiv g\theta^{-1} \gamma H^4 (\kappa \nu)^{-1}$ is the Rayleigh number, and $\sigma \equiv \nu/\kappa$ is the eddy Prandtl number (assumed to be 1).

In terms of η, v, φ' and ψ , the boundary conditions are

$$\left. \begin{aligned} \psi = \frac{\partial \psi}{\partial z} - K \frac{\partial^2 \psi}{\partial z^2} = v - K \frac{\partial v}{\partial z} = 0, \quad \varphi' = 1 & \quad \text{at } z = 0 \\ \psi = \frac{\partial^2 \psi}{\partial z^2} = \frac{\partial v}{\partial z} = \eta = \varphi' = 0 & \quad \text{at } z = 1 \\ \psi = \frac{1}{r} \frac{\partial \psi}{\partial r} - \frac{\partial^2 \psi}{\partial r^2} = \frac{\partial v}{\partial r} - \frac{v}{r} = \eta = \frac{\partial \varphi'}{\partial r} = 0 & \quad \text{at } r = L/H \\ \psi = \frac{\partial \psi}{\partial r} = v = \eta = \frac{\partial \varphi'}{\partial r} = 0 & \quad \text{at } r = 0 \end{aligned} \right\} \quad (10)$$

We use the following initial conditions at $t = 0$:

$$\left. \begin{aligned} u \equiv w \equiv \psi \equiv \eta \equiv 0 \\ v = \Omega r \cos[A(z-1)] \end{aligned} \right\} \quad (11)$$

where A is the smallest positive root of $\cot A - KA = 0$ [i.e., each layer of the atmosphere is initially in solid body rotation but the rotation rate varies with height (except when $K = \infty$) to accommodate the bottom boundary condition].

Also

$$\varphi' = 1-z + \hat{\varphi} \cos(\pi Hr/L) \sin(\pi z) \quad (12)$$

or

$$\varphi' = \frac{\exp(5(1-z)) - 1}{\exp 5 - 1} \quad (13)$$

When $\hat{\varphi} \neq 0$, we choose it positive as then the initial radial temperature gradient is negative and fluid starts rising on the axis and sinking at the outer rim. Equation (12) represents a sinusoidal disturbance imposed on a constant potential lapse rate atmosphere. Equation (13) models an atmosphere with an initial exponential stratification, and takes partial account of the strong increase of lapse rate near the ground observed under dust-devil conditions.

When $K = \infty$ (all free boundaries) the mean angular momentum of the fluid is conserved. For finite values of K it decays, but only slowly since the characteristic diffusion time, H^2/κ is large compared to the advective time scale ($\sim H/|w|$ or $L/|u|$).

It is convenient here to define a Taylor number $T \equiv 4 \Omega_d^2 H^4/\nu^2$ where Ω_d is the (dimensional) initial rate of rotation of the top surface. In terms of dimensionless quantities $T = 4 \Omega^2 R_a^2/\sigma^2$.

3. LINEARIZED SOLUTIONS

Solutions to the linearized equations can be obtained in the special case where $K = \infty$ and the basic steady state is one of solid rotation, and constant (negative) temperature gradient if we replace the boundary condition $\partial v/\partial r - v/r = 0$ at $r = L/H$ by $v = \Omega(L/H)$ (as Inman did). The solutions for perturbations from the basic state (denoted by primes) are

$$\begin{pmatrix} \varphi' \\ w' \end{pmatrix} = \begin{pmatrix} 1 \\ S_2 \\ R_a \end{pmatrix} C e^{st} J_0(kr) \sin m\pi z \quad (14)$$

$$\begin{pmatrix} u' \\ v' \end{pmatrix} = \begin{pmatrix} \frac{-m\pi S_2}{kR_a} \\ \frac{2m\pi\Omega S_2}{k R_a S_1} \end{pmatrix} C e^{st} J_1(kr) \cos m\pi z \quad (15)$$

$$\pi' = \left\{ -m\pi(S_1 S_2 + 4\Omega^2 S_2/S_1)/k^2 R_a \right\} C e^{st} J_0(kr) \cos m\pi z \quad (16)$$

where C is an arbitrary constant, $S_1 \equiv (s + \sigma k^2 + \sigma m^2 \pi^2)$, $S_2 \equiv (s + k^2 + m^2 \pi^2)$, $m = 1, 2$ etc. and k is given by the condition that kL/H are the positive zeroes of $J_1(x)$. The results are similar to those obtained by Chandrasekhār (1961) for convection in a rotating thin unbounded horizontal layer if k is replaced by horizontal wave number (continuous in his case). Chandrasekhār shows that for $\sigma \geq 1$ there are no overstable modes. This is reassuring (although it may not be true for other boundary conditions) since the phase speeds of overstable modes, if comparable to the particle velocities, would further restrict the size of the time increment in the numerical integration. For $\sigma = 1$, the growth rate is given by

$$s = \pm \sqrt{\frac{R_a k^2 - m^2 \pi^2 T}{k^2 + m^2 \pi^2} - k^2 - m^2 \pi^2} \quad \text{or} \quad -k^2 - m^2 \pi^2.$$

and a given mode is unstable if

$$R_a k^2 - m^2 \pi^2 T > (k^2 + m^2 \pi^2)^3.$$

Note that the rate of conversion of meridional into zonal kinetic energy, $-2\pi R_a \iint u'v'^2 dr dz$, is positive for $s > 0$. The ratio, $-R_a \iint u'v'^2 dr dz / \sigma \iint r w' \varphi' dr dz$, varies as T/R_a^3 and is explicitly independent of s when $\sigma = 1$. Thus, a larger fraction of potential energy is converted into zonal kinetic energy (via the meridional circulation) at higher Taylor or lower Rayleigh number.

Equation (16) shows that for $C > 0$ (i.e., those modes with hot fluid rising off the bottom at the axis), swirl enhances the initial tendency toward falling pressure at the foot of the axis.

4. NUMERICAL METHOD

To avoid 'non-linear instability' in the numerical computations, the Jacobian terms must be formulated by a second order scheme which conserves at least one quadratic quantity (Arakawa, 1966). We use Arakawa's scheme which is devised for a regular square (or rectangular with a simple generalization) mesh and conserves the following four properties of the Jacobian for a closed system (i.e., $\psi = 0$ on boundaries): $J_{rz}(a,b) + J_{rz}(b,a) = \langle J_{rz}(a,\psi) \rangle = \langle a J_{rz}(a,\psi) \rangle = \langle \psi J_{rz}(a,\psi) \rangle = 0$ where the angular brackets denote mean value over a radial cross-section of the cylinder. From (6) - (8) we see that our finite difference forms of the Jacobians conserve the cross-sectional mean of η , a radially weighted mean of η^2 , and volume means of φ^1 , $\varphi^1{}^2$, vr (angular momentum), $v^2 r^2$ and meridional kinetic energy ($-\frac{1}{2} \langle \psi \eta \rangle$) as well as other quadratic quantities with less obvious physical interpretations. In contrast, Williams (1967) and Leslie (1971) write the term $\frac{1}{r^2} J(vr,\psi)$ in (7) as $\frac{1}{r} J(v,\psi) - \frac{\partial \psi}{\partial z} \frac{v}{r^2}$ and conserve zonal velocity and zonal kinetic energy instead of angular momentum. [They also use schemes for $J(v,\psi)$ and $J(\varphi^1,\psi)$ which satisfy only two integral constraints (the physically obvious ones) and do not conserve the anti-symmetry property of the Jacobian.]

If the forcing and diffusion terms are ignored, all three prognostic equations are of the form

$$\frac{\partial \alpha}{\partial t} = J_{rz}(a,\psi)$$

where

$$J_{rz}(a,\psi) = \frac{\partial a}{\partial z} \frac{\partial \psi}{\partial r} - \frac{\partial a}{\partial r} \frac{\partial \psi}{\partial z}.$$

Consider the transformation of co-ordinates from (r,z) to (R,Z) where $R = R(r,z)$ and $Z = Z(r,z)$. From elementary properties of Jacobians we have that

$$J_{rz}(a,\psi) = J_{RZ}(a,\psi) \frac{\partial(R,Z)}{\partial(r,z)}.$$

The transformation is always chosen so that in (R,Z) -space we have a regular, square mesh of points. Consequently, it is possible to use Arakawa's scheme for $J_{RZ}(a,\psi)$. A typical quantity that we wish to conserve is $\bar{\alpha}$ the mean RZ value of α . If A is the area and name of the region in the (r,z) -plane in which the fluid motion takes place, and if A' is the corresponding region in the (R,Z) -plane, then

$$A \frac{\partial \bar{\alpha}}{\partial t} = \iint_A J_{rz}(a, \psi) dr dz = \iint_{A'} J_{rZ}(a, \psi) \left| \frac{\partial(r, z)}{\partial(R, Z)} \right| dR dZ.$$

We shall only consider transformations such that the Jacobian of the transformation is positive, i.e., one-to-one mappings between (R,Z) and (r,z). Thus

$$A \frac{\partial \bar{\alpha}}{\partial t} = \iint_{A'} J_{RZ}(a, \psi) dR dZ.$$

But since Arakawa's scheme is being used we know that the numerical analog of this integral is zero (except, possibly, for contributions from boundary points) and thus $\bar{\alpha}$ is a constant, as required. The same method obviously applies to the other quantities of interest.

The general transformation described above allows us to cluster points anywhere in physical space. However, it is usually sufficient to cluster points into the boundary layers. Thus, in this case it will suffice to have $R = R(r)$ and $Z = Z(z)$ where $R' \equiv \frac{dR}{dr}$ and $Z' \equiv \frac{dZ}{dz}$ are positive definite. The functions R and Z should be as smooth as possible. We chose the formulae given by Schulman (1971). Since we effectively have boundary layers at the axis and on both horizontal surfaces we chose

$$Z = c_1 \left(\alpha_1 z + \tanh \frac{z}{s_1} + \tanh \frac{z-1}{s_1} + \beta_1 \right)$$

$$R = c_2 \left(\alpha_2 r + \tanh \frac{r}{s_2} + \beta_2 \right).$$

(We should also have improved the resolution at the rim since the return flow tends to concentrate there - see figure 3 for example.) The eight constants were chosen such that

$$Z(0) = 0, \quad Z(1) = 1, \quad Z'(0) = D_1, \quad Z'\left(\frac{1}{2}\right) = D_2$$

$$R(0) = 0, \quad R\left(\frac{L}{H}\right) = 1, \quad R'(0) = D_1, \quad R'\left(\frac{L}{H}\right) = D_2.$$

Two pairs of values were tried for D_1 and D_2 , viz.

$$(D_1, D_2) = (4, .4) \text{ and } (D_1, D_2) = (2, .8).$$

These will be referred to in Section 5 as "severe stretch" and "moderate stretch" cases, respectively.

We define (non-staggered) grid points by

$$R_i = (i - 1)d \quad i = 0, 1, \dots, N + 1$$

$$Z_j = (j - 1)d \quad j = 0, 1, \dots, M + 1$$

where d , the grid interval in stretch space, is chosen equal to the smallest grid interval in real space. Points with $i = 0$, $i = N+1$, $j = 0$, $j = M+1$ are exterior points used to satisfy boundary conditions. All space derivative terms apart from the Jacobians are represented by the usual three point centered difference formulae.

We use Euler's method to advance η , v and φ' through the first time step, and the leap frog scheme for all subsequent time steps. The diffusion terms are lagged one time step to avoid computational instability (Richtmyer, 1957, p. 94). Provision is made in the program for keeping Δt large without coming too close to violating the stability criteria (which are only approximate);

$$\Delta t < \text{Min} \left\{ \frac{d^2}{8\sigma}, \frac{d^2}{8} \right\}$$

$$\text{Max} \left\{ \frac{|u| + |w|}{d} \right\} \Delta t < 1$$

[ignoring the possibility that gravity-inertia oscillations, possibly of large amplitude since we do not, in general, perturb about a steady state, or overstable modes may restrict Δt still further]. We also avoid time splitting by averaging the variables over adjacent time steps every twentieth step.

Values of φ' on the axis are obtained by using L'Hôpital's rule to rewrite (8) in a form suitable for use on the axis (i.e., free from singularities). We also need to substitute $\frac{1}{r} J(\eta, \psi) + \frac{\eta}{r^2} \frac{\partial \psi}{\partial z}$ for $J(\frac{\eta}{r}, \psi)$ at points where $r = d$ since the finite difference form of $J(\frac{\eta}{r}, \psi)$ is indefinite there.

The general integration procedure is as follows. We apply the marching technique to update φ' , v and η at all interior and some boundary points. We use the boundary conditions to determine the remaining boundary values and exterior values (as needed), except for values of η along the bottom boundary which are indeterminate as yet. We update ψ by solving (9) with $\psi = 0$ on the boundaries by over-relaxation. The additional boundary conditions on ψ determine ψ at exterior points, and enable us to complete the integration by evaluating η on the bottom from (9) and the updated ψ -field.

5. RESULTS

5.1 Selection of Flow Parameters

The flow depends on the Rayleigh number, the Taylor number, the initial and boundary conditions and the aspect ratio (the Prandtl number is fixed at 1). It is practical to vary the flow parameters only through a restricted range of values. The Rayleigh number was chosen to lie between 6×10^4 and 1.2×10^6 in all cases, and was set equal to 6×10^5 in most runs. At higher Rayleigh numbers, too fine a mesh is needed to resolve the small scale motions which become increasingly important in the heat transports and Reynolds stresses. Lower Rayleigh numbers are also not practical as the meridional circulation proceeds slowly, long time integrations are necessary, and the elapsed time for vortex formation becomes comparable to the diffusion time. Furthermore, the vortices are weaker as centrifugal opposition to flow toward the axis has more effect.

The Taylor number also cannot be larger than about 10^5 as the swirl inhibits the largest-scale convection most, and at higher Taylor numbers the meridional circulation breaks down into two or more cells.

A value of one was found to be the optimum choice for the aspect ratio. We found that increasing the aspect ratio above this value had little effect on the vortex strength until the circulation broke down into two cells (at some value less than two). However, flows at smaller aspect ratios produced weaker vortices due probably to increased viscous dissipation in the fluid interior.

It would have been preferable to integrate to a (quasi-) steady state as the steady-state solutions obtained would then stand on their own merit, and little attention need be paid to the actual path to the steady state, which depends on the quite arbitrary initial conditions. Of course, different steady states might be reached from different initial conditions even for initial small perturbations away from an unstable equilibrium state as found by Ogura (1971). We found similar behavior at large K (≈ 316) where the initial state is very close to being one of unstable equilibrium, and the introduction of a small initial temperature disturbance of amplitude 0.001, was sufficient to prevent the subsequent breakdown of the flow into two cells. However, at small or zero K we are a long way from an initial equilibrium state so that a small temperature perturbation makes little difference. In addition we cannot obtain a steady state vortex without artificially prescribing v (as a function of z) on the rim and this proved unsatisfactory because of the formation of large radial shears in v near the rim (except for $K \rightarrow \infty$). Thus, the initial conditions can play a critical role in the determination of the flow, and hence of the properties of the transient vortex that forms.

We tried other kinematic boundary conditions, in addition to those already described in Section 2. In one variation (see Section 5.4) with a free bottom boundary, we fixed v on the side (after Inman) so that we could obtain a (quasi-) steady state vortex. The results were similar in structure to the transient vortex that forms in the same case when the rim is allowed to be completely free. Cases were also run where the boundary conditions were those applicable to a rotating tank with either a free or a rigid lid. These were considered unsuccessful as the meridional flow broke into two cells and the resulting steady state was complicated.

5.2 Test of Stretched Coordinate System

The case with $R_a = 6 \times 10^5$, $T = 4 \times 10^4$, $L/H = 1$ and $K = 0.01$ was chosen for testing the stretched coordinate system. In all runs a 26×26 mesh was used. In the no-stretch run the temperature contours become jagged near the axis (see figure 1). Convection tries to establish a nearly isothermal core on the axis such that the isotherms there are vertical. However, the boundary condition is that the horizontal temperature gradient is zero; i.e., that the isotherms are horizontal. This situation causes numerical problems which produce the jaggedness; also it is noticeable that the spikes get worse in the direction of the flow. One consequence of these spikes is that the temperature gets as high as 1.2, which is clearly unphysical since the boundary temperatures are fixed at 0 and 1. These numerical difficulties do not seem to have any other serious results, probably because they do not appear until close to the time when v is reaching its maximum, and the integration is stopped soon after this point.

In the severe-stretched system the situation is worse. Now the spikes are much broader, smoother and bigger and appear sooner. Thus, the whole flow is affected and there is very poor agreement with the unstretched system. Again, the temperature goes up to about 1.2. Spikes also begin growing from the top boundary in the v -field. Another disquieting feature is that there are small oscillations of about 100 time steps in the flow. This system is also uneconomical since the diffusion time-step limit is cut by a factor of 16 from the unstretched case (because the smallest grid interval is decreased by a factor 4).

With the moderate-stretch system, however, there are definite improvements over a square mesh³ as shown by figure 2. There are now no spikes and the temperature does not exceed 1. The η -field is also much smoother than in the other cases. Otherwise, there is generally good agreement with the square-mesh case. We attribute these results to the fact that too severe a stretching, although it improves radial

3 Note that the moderate-stretch 26×26 grid has the same resolution near the axis and horizontal boundaries as a 51×51 square mesh, but is much more economical, and, was found to achieve comparable results.

resolution near the axis, makes the vertical resolution poor there at the mid-levels. It would appear from these experiments that considerable care is required in choosing the stretching if the best possible results are to be obtained.

5.3 Case with Rigid Bottom Surface ($K = 0$)

We choose the case, $R_a = 6 \times 10^5$, $T = 4 \times 10^4$, $L/H = 1$, $\hat{\phi} = K = 0$ with the initial conditions (11)^a and (12) and the boundary conditions (10), to describe in detail. We used moderate stretching with a 26x26 grid. Initially, the meridional circulation is uni-cellular with maximum up-draft, downdraft, outflow and inflow at the axis, rim, top and $z \sim 0.11$, respectively. By $t = 1.18 \times 10^{-2}$ a plume of hot fluid rising along and near the axis has hit the top surface, and spread out laterally, forming in the process a very strong thermal boundary layer along the top. The cold downdraft descending at the rim also forms a thermal boundary layer along the outer part of the bottom surface, but this layer is not as thin. The inflow has drawn the vortex lines in to form a diffuse vortex with a nearly isothermal core. At this stage the maximum updraft is about 0.2 radii from the axis. By $t = 1.38 \times 10^{-2}$ it is back on the axis, the center of the streamline pattern has lowered but the inflow layer is still relatively thick ($\sim .25$). The point of maximum swirl is located at $r = .19$, $z = .62$, and the radius of the isothermal core has decreased considerably.

The vortex reaches its maximum intensity at $t = 1.49 \times 10^{-2}$. The swirl amplification factor, S , defined in the introduction, is 2.77 and the maximum tangential velocity, v_{\max} , is located at $r_{\max} = .13$, $z_{\max} = .67$. Figures 3, 4, and 5 show the stream function, zonal velocity and temperature fields at this time. A notable feature is the appearance of a region of weak flow reversal in the ground boundary layer. This is probably due to an adverse pressure gradient associated with deceleration of the inflow⁴. In fact, the whole region near the bottom of the axis is one of relatively weak flow, and the streamline pattern suggests that the vortex is not in contact with the ground.

We can justify our neglect of density variations in the centrifugal force by noting from our results that the ratio of maximum centrifugal acceleration to gravitational acceleration (a rotational Froude number),

$$R_a \frac{\gamma H}{\theta} \text{Max}_{r,z,t} \left[\frac{v_*^2}{r_*} \right] \leq \frac{\gamma H}{\theta} \ll 1.$$

4 Ward (1970) notes that barograph recordings of tornado passages frequently show high pressure rings surrounding the core, and is able to obtain similar surface pressure profiles with his laboratory model at low inflow angles. With increasing rotation, the ring disappears as the flow above the boundary layer becomes more cyclostrophic.

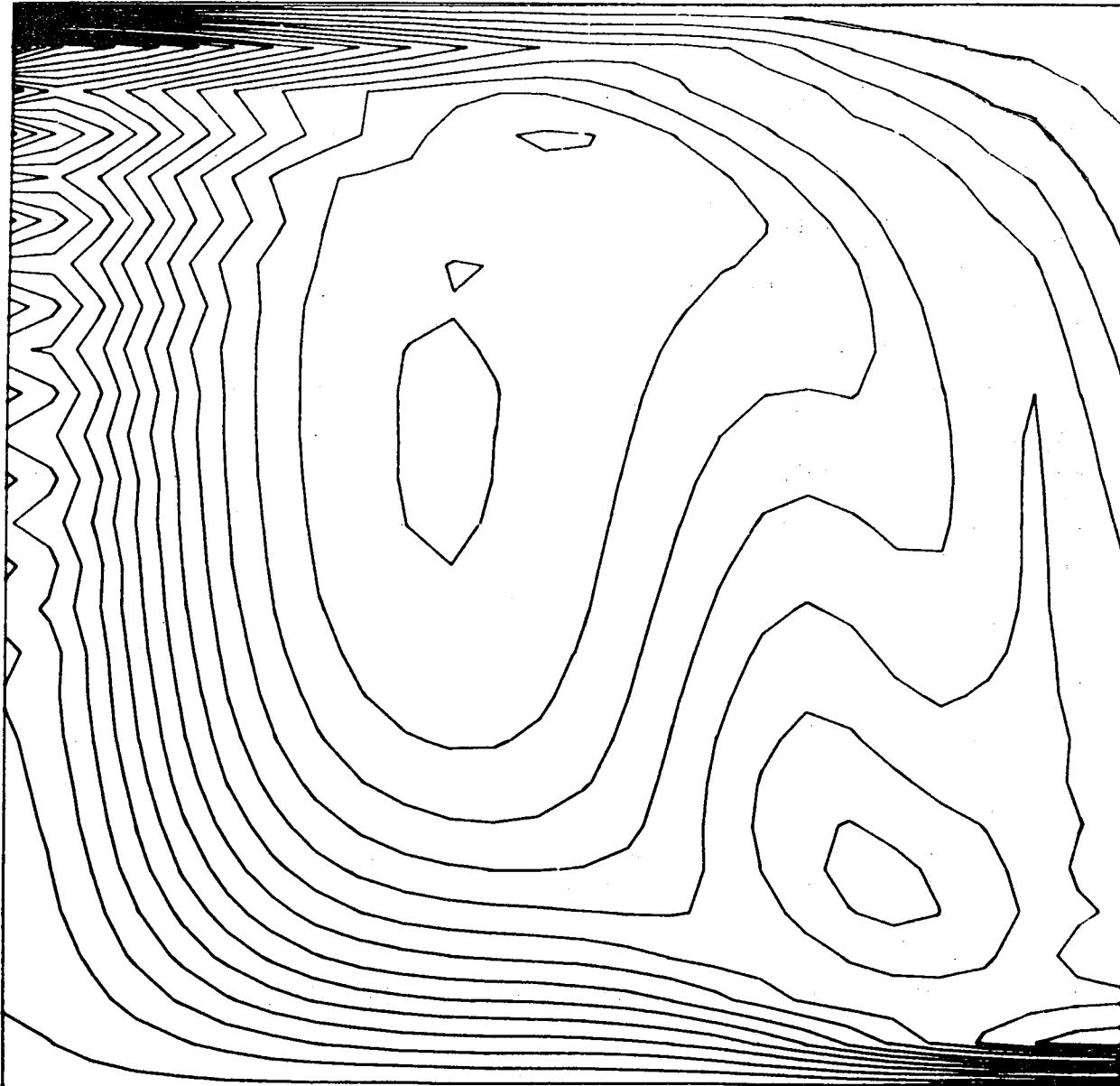


Figure 1. Temperature field at $t = 1.54 \times 10^{-2}$ with square 26x26 mesh, illustrating spikes in isotherms near axis.

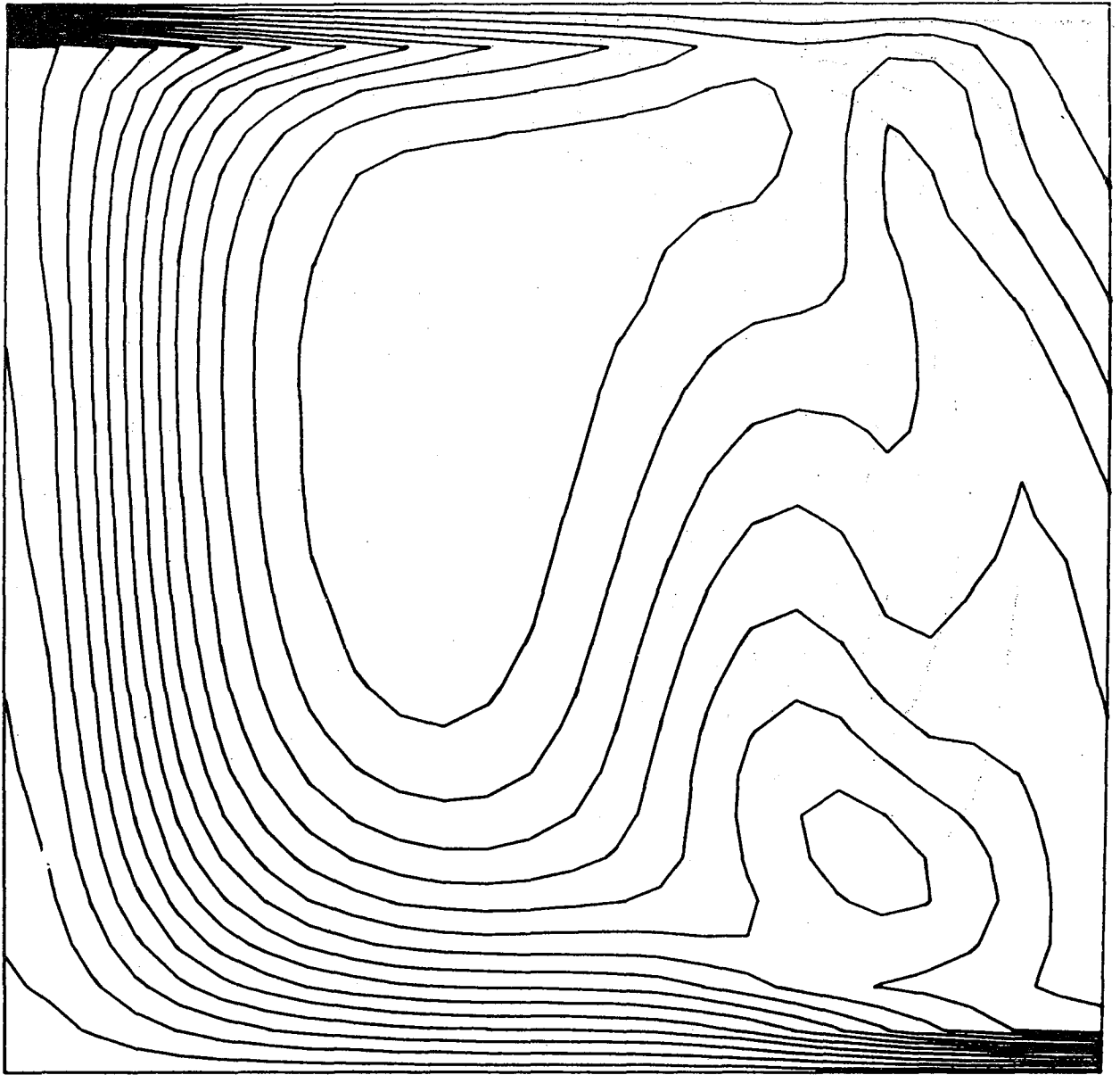


Figure 2. Isotherms at $t = 1.60 \times 10^{-2}$ in same case as figure 1, showing effect of moderate coordinate stretching in smoothing contours.

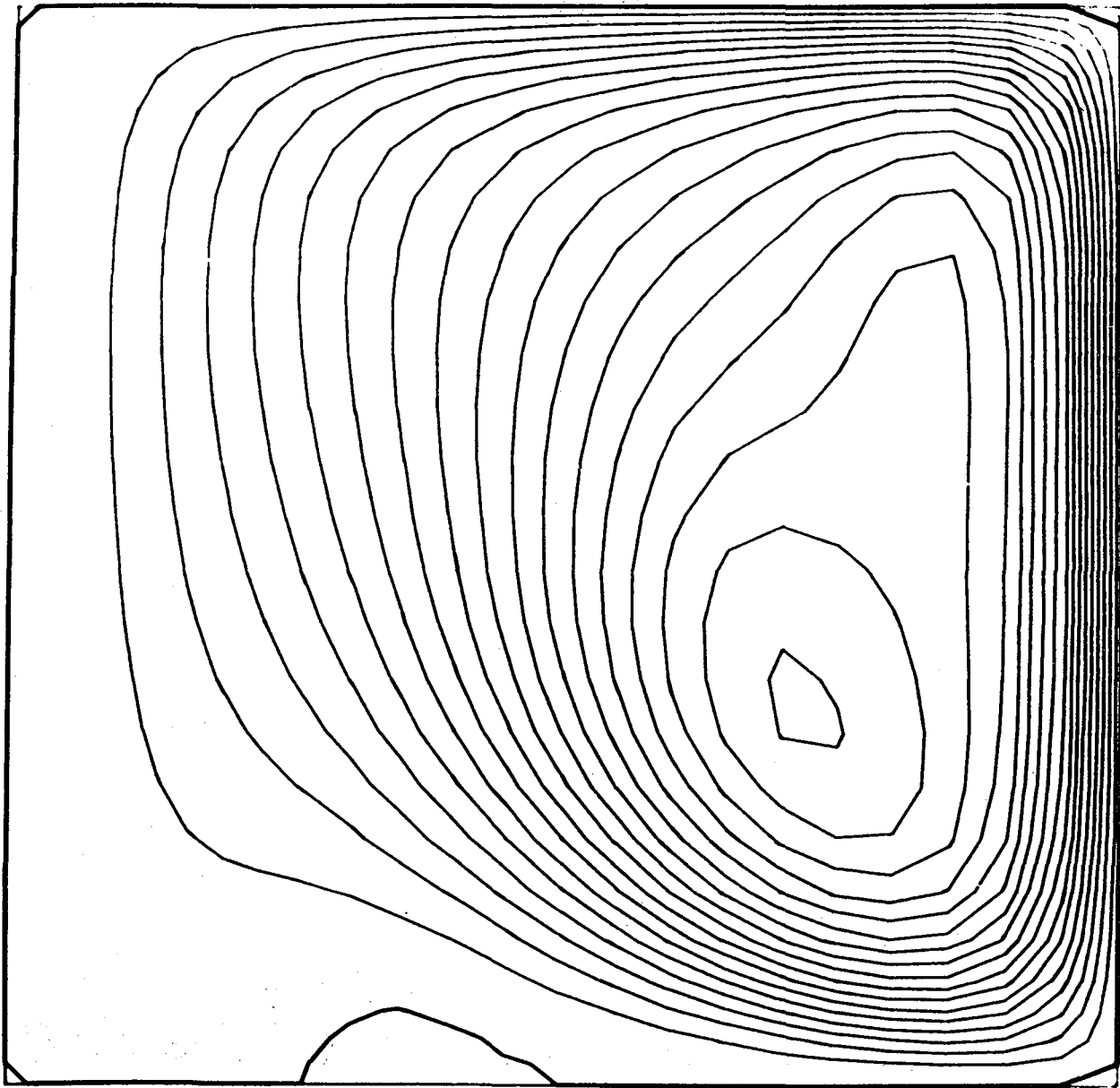


Figure 3. Streamlines at time of maximum vortex intensity for case described in Section 5.3.

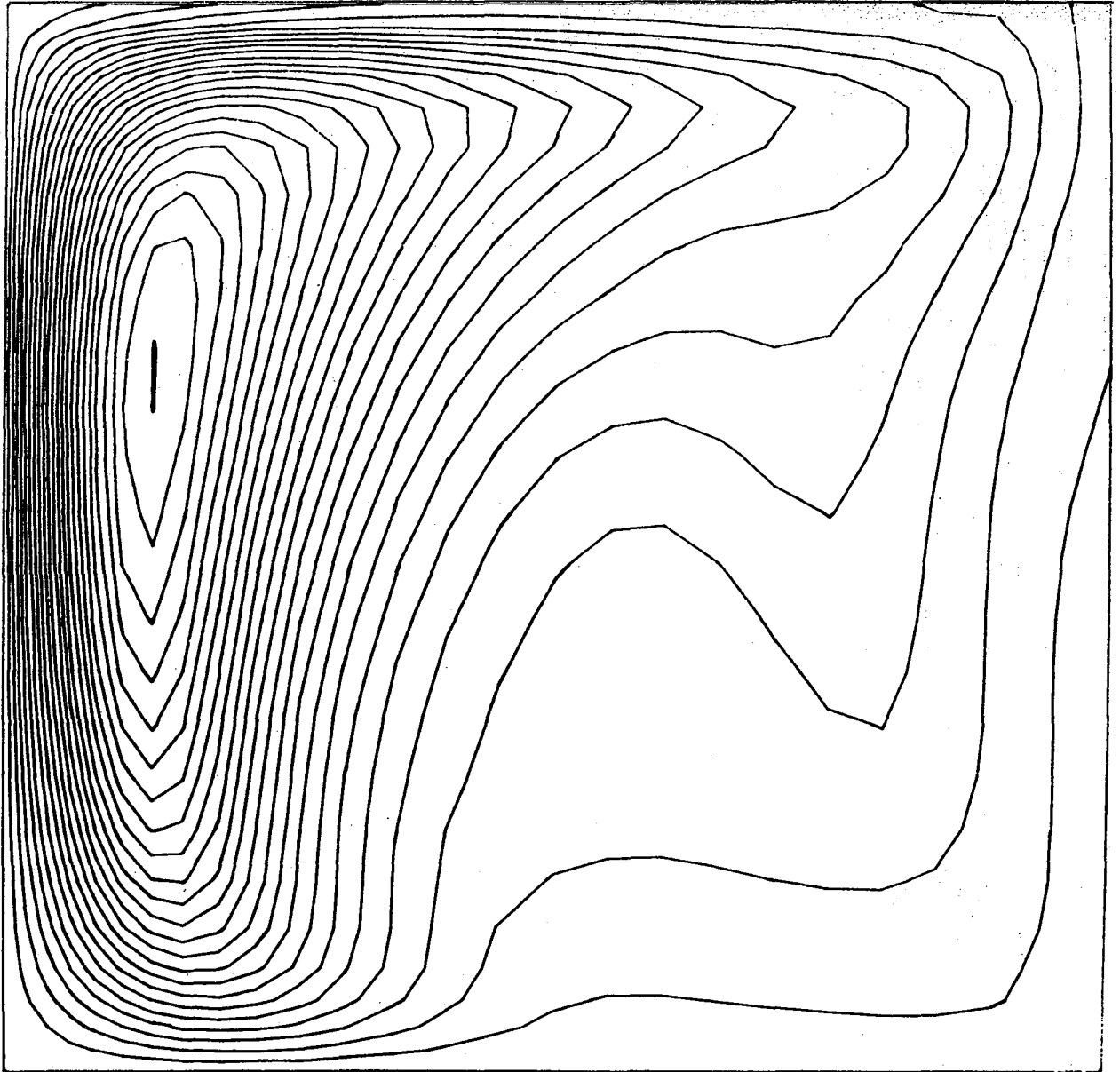


Figure 4. Contours of zonal velocity at time of maximum vortex intensity for case described in Section 5.3.

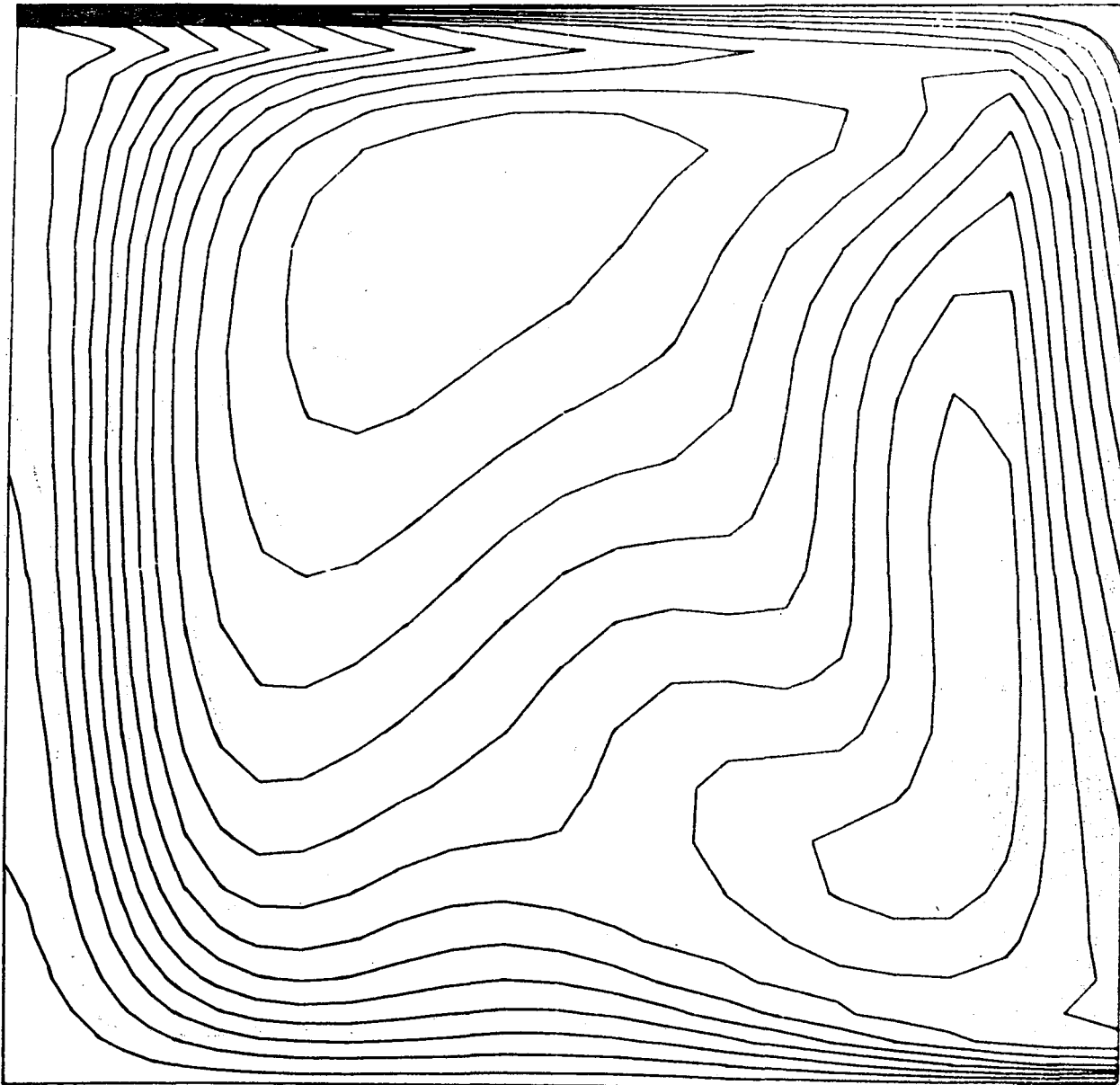


Figure 5. Isotherms at time of maximum vortex intensity for case described in Section 5.3.

The intensity of the vortex subsequently decays in an oscillatory fashion, and the flow reversal disappears by $t = 2 \times 10^{-2}$. At the time of maximum intensity the fluid has lost only about 20% of its original mean angular momentum to the ground.

We ran a similar case with zero swirl except for an initial temperature wave of amplitude $\phi = .001$, which was necessary to perturb the system. This flow also exhibited strong downflow on the rim and strong vertical temperature gradients near the top surface and the foot of the rim. The weak flow reversal appeared at the same place but at a later time ($t \sim 2 \times 10^{-2}$). The maximum updraft was always on the axis, and the meridional circulation was roughly the same strength as in the swirl case. It thus appears that at $T = 2 \times 10^4$ there is not very close coupling between the axial and azimuthal flow even though the ratio of characteristic zonal and vertical velocities for the vortex is about 0.4. (Leslie claims there will be close coupling if this ratio is of order one.)

5.4 Case with Free Bottom Surface

We will also describe the case, $R_a = 6 \times 10^5$, $T = 2304$, $L/H = 1$, $\phi = 0.001$, $K = \infty$ (i.e., free bottom) with the initial conditions (11) and (12), and the same boundary conditions as (10) except that v was fixed at the outer rim so that a quasi-steady state vortex solution could be obtained. We used a lower Taylor number here than in the previous cases because the meridional flow no longer consists of a single cell at $T = 4 \times 10^4$. These computations were performed on a 26×26 grid without stretching.

The effect of 'freeing' the lower surface is quite dramatic. The vortex becomes greatly more concentrated and makes contact with the ground due to inflow along the bottom. Figures 6, 7, and 8 show the quasi-steady state solutions for ψ , v and ϕ' (at $t = 2.16 \times 10^{-2}$). The maximum swirl occurs at the ground and the first grid point away from the axis, so clearly a finer grid should have been used to resolve the core. The swirl amplification factor is about 13, and the assumption that we can neglect density variations in the centrifugal force is now a bad one in the vicinity of the vortex core. However, a centrifugal circulation would enhance the one cell meridional circulation, and hence the vortex. Deformation of the top surface should also occur at rotational Froude numbers of order one or larger and should again aid vortex formation by lowering pressure on the axis if we assume that potentially lighter fluid lies above the top surface. The maximum updraft always lies on or very close to the axis, and the inflow is a minimum at the bottom.

A similar case was run with $T = 0$, and again shows that the swirl has little inhibiting effect on the convection at $T = 2304$. Therefore, the fact that we get a more concentrated vortex when we free the bottom surface can be attributed to inflow along the ground. Presumably, in more rotation dominated flows the no-slip condition is more favorable for

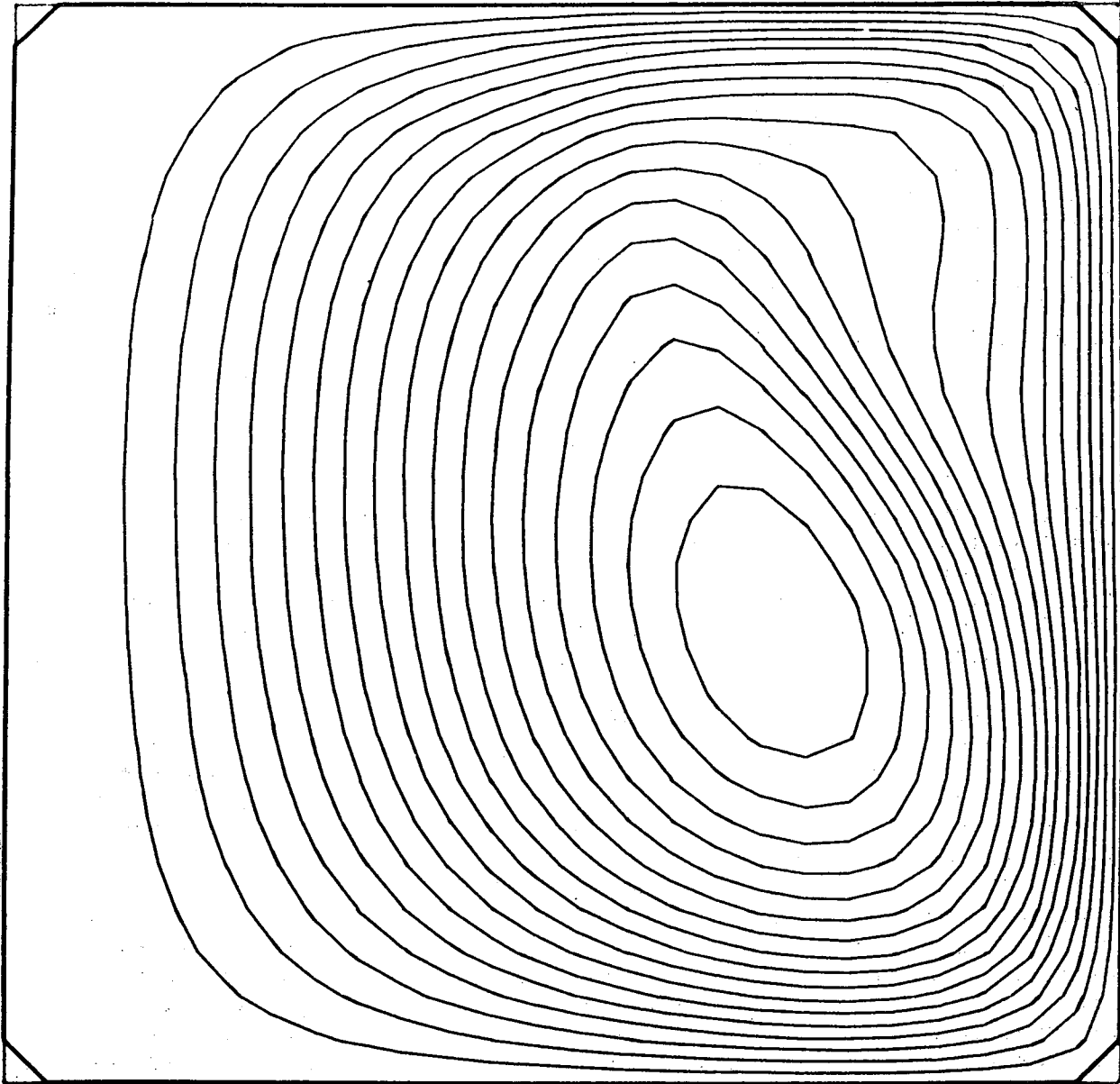


Figure 6. Streamlines at quasi-steady state for case described in Section 5.4.

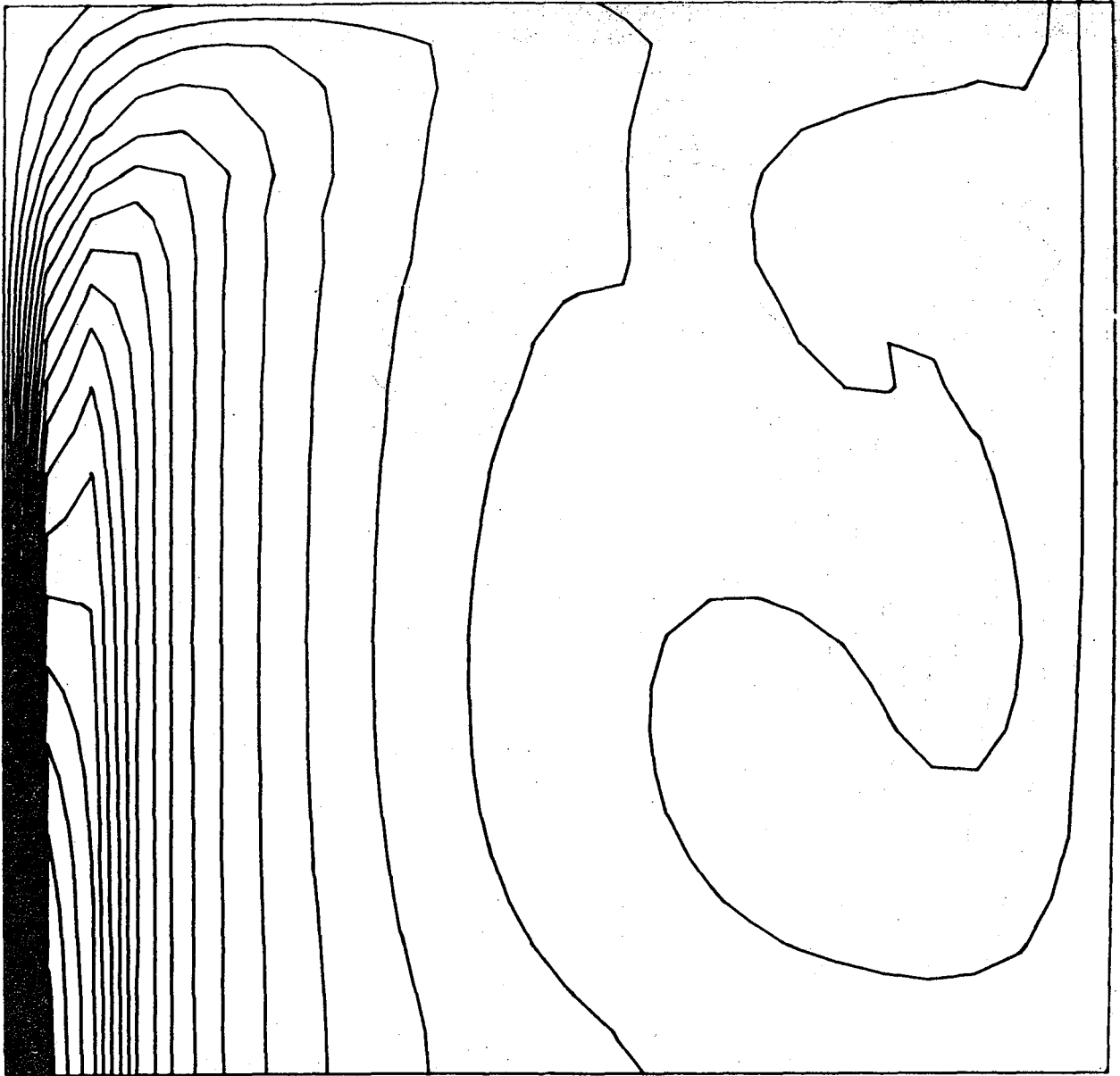


Figure 7. Contours of zonal velocity at quasi-steady state for case described in Section 5.4.

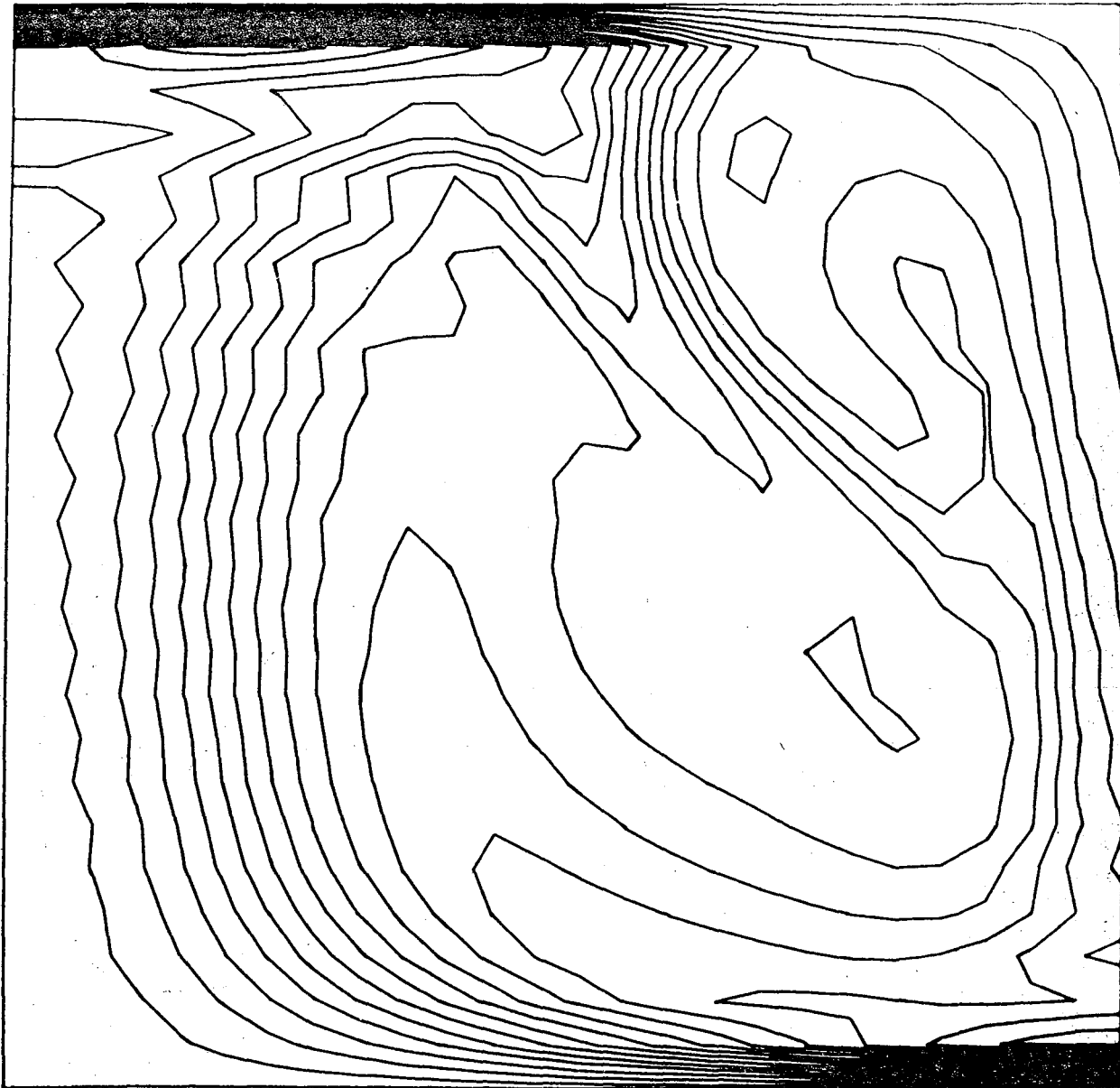


Figure 8. Isotherms at quasi-steady state for case described in Section 5.4.

vortex formation because the centrifugal force and pressure gradient balance in the fluid interior and friction is required to allow inflow near the ground.

We also ran a similar case at $T = 2304$ with a completely free rim. The flow was very similar, except that the vortex was transient, rather than steady, but it was almost as intense. In this case mean angular momentum of the fluid should be conserved as all the boundaries are free. We were able to verify that our numerical scheme conserved this quantity to within 0.5% during the run.

5.5 Effects of Varying Flow Parameters

A 26x26 regularly spaced grid was used in all cases described in this section for $R_a < 10^6$. At higher Rayleigh numbers the grid was 51x51 with moderate stretching. The meridional circulation apparently always starts out as one cell.

Increasing the Rayleigh number over the range 3×10^5 to 1.2×10^6 (with $T = 4 \times 10^4$, $L/H = 1$, $K = .01$ and the exponential initial temperature profile (13)) increases S from 2.2 to 3.4 and decreases r_{\max} by about 50% to 0.08. This is probably due to the increasing meridional circulation. However, when we further increase R_a to 4.8×10^6 a two-cell flow develops.

For $R_a = 6 \times 10^5$, $L/H = 1$, $K = 0$ and $\varphi' = 1 - z$ initially, the Taylor number was varied from 23 to 2×10^6 . Over a surprisingly large range of T (from $\sim 2 \times 10^3$ to 2×10^5) the maximum strength of the vortex was constant with $S \sim 2.6$, $r_{\max} \sim .16$ and $z_{\max} \sim .68$. At higher Taylor numbers the flow split into two cells due to the effect of rotation on the convection. However, two cells also developed at low Taylor numbers. The reason for this is not apparent to us (especially since with $T = 0$, $\hat{\varphi} = .001$ the flow is one cell except for a small flow reversal next to the ground for $t < 2.3 \times 10^{-2}$).

Changing from the linear to the exponential initial temperature profile did not affect the strength of the subsequent vortex very much, but in the early stages before a strong vortex developed the flow was 'buffered' from the top surface by a stable region. Strong temperature gradients developed at the base of the stable region instead of at the top surface.

More concentrated vortices are produced when the no-slip condition on the bottom is relaxed (i.e., when K is increased through the range 0 to ∞), unless two-cell breakdown occurs in the process (which it does for $R_a = 6 \times 10^5$, $T = 4 \times 10^4$, $L/H = 1$). Table 1 shows how S and the location and time of maximum swirl vary with K for $R_a = 6 \times 10^5$, $T = 2304$, $L/H = 1$, $\hat{\varphi} = .001$. However, we should really have had more resolution for $K > .3$, as the maximum swirl is located only one grid point away from the axis in these cases. The point of maximum tangential velocity approaches the

axis and the surface as K is increased, but the time of maximum vortex development does not change significantly (perhaps due to smaller initial disturbance balancing decreased dissipation).

TABLE 1

S , r_{\max} , z_{\max} and t_{\max} as a function of K for $R_a = 6.10^5$,

$T = 2304$, $L/H = 1$, $\hat{\phi} = 0.001$

K	S	r_{\max}	z_{\max}	$t_{\max} \times 10^{-2}$
0	2.6	.16	.68	1.94
.01/10	3.2	.12	.68	1.85
.1	4.5	.08	.52	1.84
.1/10	6.9	.08	.28	1.79
1	9.6	.04	.04	1.78
$\sqrt{10}$	11.3	.04	.04	1.79
10	11.9	.04	0	1.80
∞	12.3	.04	0	1.81

6. CONCLUSIONS

We have demonstrated that vortices as intense as those obtained by Leslie can be generated after replacing his externally supplied buoyancy with thermal buoyancy. However, allowing advection and diffusion of buoyancy makes it much more difficult to demonstrate the same effects as Leslie. For instance, our vortices apparently do not make contact with a no-slip bottom surface. They also do not grow down from the top, although this is probably caused by application of the buoyancy force only at the top one third of the axis in Leslie's model. We get strong downdrafts near the rim whereas Leslie only gets weak down flows. The

rotation does not restrict the radial inflow much to the bottom boundary layer, and freeing a horizontal surface (the bottom here, the top in Leslie's work) produces a stronger rather than weaker vortex. We can deduce from these results that in our experiments rotation does not inhibit the convection very much and we do not have a centrifugal force-pressure gradient balance in the interior of the fluid. However, we are unable to increase the rotation further without getting complicated multi-cellular flows.

Our work also suffers, as far as atmospheric applications are concerned, from the flow being contained in a closed box and from the presence of isothermal top and bottom surfaces which cause strong thermal boundary layers to form. Other, less restrictive, boundary conditions are clearly needed. Also, it is difficult to handle the effects of atmospheric turbulence with any degree of realism in the neighborhood of a developing vortex.

7. ACKNOWLEDGMENTS

The authors are grateful to the Advanced Study Program of the National Center for Atmospheric Research for support provided during the course of this study. We also wish to thank Dr. J. W. Deardorff and Dr. J. O'Brien for helpful discussions. We are further indebted to the National Center for Atmospheric Research for computer time on the CDC 6600 and 7600 machines used in this research.

8. REFERENCES

- Arakawa, A., 1966: Computational design for long term numerical integration of the equations of fluid motion. Two-dimensional incompressible flow. Part 1. J. Comput. Phys. 1, 119-143.
- Barcilon, A. I., 1967: A theoretical and experimental model for a dust devil. J. Atmos. Sci. 24, 453-466.
- Burgers, J. M., 1948: A mathematical model illustrating the theory of turbulence. Adv. in Appl. Mech., Vol. 1, Academic Press, New York.
- Chandrasekhar, S., 1961: Hydrodynamic and hydromagnetic stability. Clarendon Press, Oxford 652 pp.
- Gutman, L. N., 1957: Theoretical model of a waterspout. Bull. Acad. of Sciences, USSR (Geophysical Series), New York, Pergamon Press translation, 87-103.
- Inman, R. L., 1966: The evolution of convective motions in a rotating fluid. Ph. D. Thesis, Texas A&M University, 90 pp.
- Kuo, H. L., 1966: On the dynamics of convective atmospheric vortices. J. Atmos. Sci. 23, 25-42.
- Kuo, H. L., 1971: Axisymmetric flows in the boundary layer of a maintained vortex. J. Atmos. Sci., 28, 20-41.
- Leslie, L. M., B. R. Morton, and R. K. Smith, 1970: On modelling tornadoes. Quart. J. Roy. Met. Soc., 96, 544-548.
- Leslie, L. M., 1971: The development of concentrated vortices: a numerical study. J. Fluid Mech., 48, 1-21.
- Lilly, D. K., 1969: Tornado Dynamics. NCAR Manuscript 69-117, National Center for Atmospheric Research, Boulder, Colorado.
- Long, R. R., 1956: Sources and sinks at the axis of a rotating liquid. Quart. J. Mech. Appl. Math., 9, 385-393.
- Long, R. R., 1958: Vortex motion in a viscous fluid. J. Meteor. 15, 108-112.
- Ogura, Y. and N. A. Phillips, 1962: Scale analysis of deep and shallow convection in the atmosphere. J. Atmos. Sci., 19, 173-179.
- Ogura, Y., 1963: The evolution of a moist convective element in a shallow, conditionally unstable atmosphere: a numerical calculation. J. Atmos. Sci., 20, 407-424.

- Ogura, Y., 1971: A numerical study of wavenumber selection in finite amplitude Rayleigh convection. J. Atmos. Sci., 28, 709-717.
- Richtmyer, R. D., 1957: Difference methods for initial value problems. New York: Interscience, 238 pp.
- Ryan, J. A., and J. J. Carroll, 1970: Dust devil wind velocities: mature state. J. Geophys. Res., 75, 531-541.
- Schulman, E. E., 1970: Antarctic circumpolar current. Proceedings of Computer Simulation Conference, Denver, Colorado, June 6-12, 1970, pp 955-968. A.C.M./S.H.A.R.E./S.C.I.
- Serrin, J., 1971: The swirling vortex. Report from the School of Mathematics, University of Minnesota. To appear in Phil. Trans. Roy. Soc. London, Series A.
- Sullivan, R. D., 1959: A two-cell vortex solution of the Navier-Stokes equations. J. of the Aerospace Sciences, 26, 767-768.
- Turner, J. S. and D. K. Lilly, 1963: The carbonated-water tornado vortex. J. Atmos. Sci., 20, 468-471.
- Turner, J. S., 1966: The constraints imposed on tornado-like vortices by the top and bottom boundary conditions. J. Fluid Mech. 25, 377-400.
- Ward, N. B., 1970: The exploration of certain features of tornado dynamics using a laboratory model. NOAA Technical Memorandum ERLTM-NSSL 52, National Severe Storms Laboratory, Norman, Oklahoma.
- Wilkins, E. M., Y. Sasaki and R. H. Schauss, 1971: Vortex formation by successive thermals: A numerical simulation. Mon. Wea. Rev., 99, 577-592.
- Williams, G. P., 1967: Thermal convection in a rotating fluid annulus: Part 1. The basic axisymmetric flow. J. Atmos. Sci., 24, 144-161.
- Wippermann, R., L. Berkofsky and A. Szillinsky, 1969: Numerical experiments on the formation of a tornado funnel under an intensifying vortex. Quart. J. Roy. Met. Soc., 95, 689-702.
- Ying, S. J., and C. C. Chang, 1970: Exploratory model study of tornado-like vortex dynamics. J. Atmos. Sci. 27, 3-14.

NATIONAL SEVERE STORMS LABORATORY

The NSSL Technical Memoranda, beginning with No. 28, continue the sequence established by the U. S. Weather Bureau National Severe Storms Project, Kansas City, Missouri. Numbers 1-22 were designated NSSL Reports. Numbers 23-27 were NSSL Reports, and 24-27 appeared as subseries of Weather Bureau Technical Notes. These reports are available from the National Technical Information Service, Operations Division, Springfield, Virginia 22151, for \$3.00, and a microfiche version for \$0.95. NTIS numbers are given below in parentheses.

- No. 1 National Severe Storms Project Objectives and Basic Design. Staff, NSSL. March 1961. (PB-168207)
- No. 2 The Development of Aircraft Investigations of Squall Lines from 1956-1960. B. B. Goddard. (PB-168208)
- No. 3 Instability Lines and Their Environments as Shown by Aircraft Soundings and Quasi-Horizontal Traverses. D. T. Williams. February 1962. (PB-168209)
- No. 4 On the Mechanics of the Tornado. J. R. Fulks. February 1962. (PB-168210)
- No. 5 A Summary of Field Operations and Data Collection by the National Severe Storms Project in Spring 1961. J. T. Lee. March 1962. (PB-165095)
- No. 6 Index to the NSSL Surface Network. T. Fujita. April 1962. (PB-168212)
- No. 7 The Vertical Structure of Three Dry Lines as Revealed by Aircraft Traverses. E. L. McGuire. April 1962. (PB-168213)
- No. 8 Radar Observations of a Tornado Thunderstorm in Vertical Section. Ralph J. Donaldson, Jr. April 1962. (PB-174859)
- No. 9 Dynamics of Severe Convective Storms. Chester W. Newton. July 1962. (PB-163319)
- No. 10 Some Measured Characteristics of Severe Storms Turbulence. Roy Steiner and Richard H. Rhyne. July 1962. (N62-16401)
- No. 11 A Study of the Kinematic Properties of Certain Small-Scale Systems. D. T. Williams. October 1962. (PB-168216)
- No. 12 Analysis of the Severe Weather Factor in Automatic Control of Air Route Traffic. W. Boynton Beckwith. December 1962. (PB-168217)
- No. 13 500-Kc./Sec. Sferics Studies in Severe Storms. Douglas A. Kohl and John E. Miller. April 1963. (PB-168218)
- No. 14 Field Operations of the National Severe Storms Project in Spring 1962. L. D. Sanders. May 1963. (PB-168219)
- No. 15 Penetrations of Thunderstorms by an Aircraft Flying at Supersonic Speeds. G. P. Roys. Radar Photographs and Gust Loads in Three Storms of 1961 Rough Rider. Paul W. J. Schumacher. May 1963. (PB-168220)
- No. 16 Analysis of Selected Aircraft Data from NSSL Operations, 1962. T. Fujita. May 1963. (PB-168221)
- No. 17 Analysis of Methods for Small-Scale Surface Network Data. D. T. Williams. August 1963. (PB-168222)
- No. 18 The Thunderstorm Wake of May 4, 1961. D. T. Williams. August 1963. (PB-168223)
- No. 19 Measurements by Aircraft of Condensed Water in Great Plains Thunderstorms. George P. Roys and Edwin Kessler. July 1966. (PB-173048)
- No. 20 Field Operations of the National Severe Storms Project in Spring 1963. J. T. Lee, L. D. Sanders and D. T. Williams. January 1964. (PB-168224)
- No. 21 On the Motion and Predictability of Convective Systems as Related to the Upper Winds in a Case of Small Turning of Wind with Height. James C. Fankhauser. January 1964. (PB-168225)
- No. 22 Movement and Development Patterns of Convective Storms and Forecasting the Probability of Storm Passage at a Given Location. Chester W. Newton and James C. Fankhauser. January 1964. (PB-168226)
- No. 23 Purposes and Programs of the National Severe Storms Laboratory, Norman, Oklahoma. Edwin Kessler. December 1964. (PB-166675)
- No. 24 Papers on Weather Radar, Atmospheric Turbulence, Sferics, and Data Processing. August 1965. (AD-621586)
- No. 25 A Comparison of Kinematically Computed Precipitation with Observed Convective Rainfall. James C. Fankhauser. September 1965. (PB-168445).

- No. 26 Probing Air Motion by Doppler Analysis of Radar Clear Air Returns. Roger M. Lhermitte. May 1966. (PB-170636)
- No. 27 Statistical Properties of Radar Echo Patterns and the Radar Echo Process. Larry Armijo. May 1966. The Role of the Kutta-Joukowski Force in Cloud Systems with Circulation. J. L. Goldman. May 1966. (PB-170756)
- No. 28 Movement and Predictability of Radar Echoes. James Warren Wilson. November 1966. (PB-173972)
- No. 29 Notes on Thunderstorm Motions, Heights, and Circulations. T. W. Harrold, W. T. Roach, and Kenneth E. Wilk. November 1966. (AD-644899)
- No. 30 Turbulence in Clear Air Near Thunderstorms. Anne Burns, Terence W. Harrold, Jack Burnham, and Clifford S. Spavins. December 1966. (PB-173992)
- No. 31 Study of a Left-Moving Thunderstorm of 23 April 1964. George R. Hammond. April 1967. (PB-174681)
- No. 32 Thunderstorm Circulations and Turbulence from Aircraft and Radar Data. James C. Fankhauser and J. T. Lee. April 1967. (PB-174860)
- No. 33 On the Continuity of Water Substance. Edwin Kessler. April 1967. (PB-175840)
- No. 34 Note on the Probing Balloon Motion by Doppler Radar. Roger M. Lhermitte. July 1967. (PB-175930)
- No. 35 A Theory for the Determination of Wind and Precipitation Velocities with Doppler Radars. Larry Armijo. August 1967. (PB-176376)
- No. 36 A Preliminary Evaluation of the F-100 Rough Rider Turbulence Measurement System. U. O. Lappe. October 1967. (PB-177037)
- No. 37 Preliminary Quantitative Analysis of Airborne Weather Radar. Lester P. Merritt. December 1967. (PB-177188)
- No. 38 On the Source of Thunderstorm Rotation. Stanley L. Barnes. March 1968. (PB-178990)
- No. 39 Thunderstorm - Environment Interactions Revealed by Chaff Trajectories in the Mid-Troposphere. James C. Fankhauser. June 1968. (PB-179659)
- No. 40 Objective Detection and Correction of Errors in Radiosonde Data. Rex L. Inman. June 1968. (PB-180284)
- No. 41 Structure and Movement of the Severe Thunderstorms of 3 April 1964 as Revealed from Radar and Surface Mesonet Data Analysis. Jess Charba and Yoshikazu Sasaki. October 1968. (PB-183310)
- No. 42 A Rainfall Rate Sensor. Brian E. Morgan. November 1968. (PB-183979)
- No. 43 Detection and Presentation of Severe Thunderstorms by Airborne and Ground-Based Radars: A Comparative Study. Kenneth E. Wilk, John K. Carter, and J. T. Dooley. February 1969. (PB-183572)
- No. 44 A Study of a Severe Local Storm of 16 April 1967. George Thomas Haglund. May 1969. (PB-184-970)
- No. 45 On the Relationship Between Horizontal Moisture Convergence and Convective Cloud Formation. Horace R. Hudson. March 1970. (PB-191720)
- No. 46 Severe Thunderstorm Radar Echo Motion and Related Weather Events Hazardous to Aviation Operations. Peter A. Barclay and Kenneth E. Wilk. June 1970. (PB-192498)
- No. 47 Evaluation of Roughness Lengths at the NSSL-WKY Meteorological Tower. Leslie D. Sanders and Allen H. Weber. August 1970. (PB-194587)
- No. 48 Behavior of Winds in the Lowest 1500 ft in Central Oklahoma: June 1966 - May 1967. Kenneth C. Crawford and Horace R. Hudson. August 1970.
- No. 49 Tornado Incidence Maps. Arnold Court. August 1970. (COM-71-00019)
- No. 50 The Meteorologically Instrumented WKY-TV Tower Facility. John K. Carter. September 1970. (COM-71-00108)
- No. 51 Papers on Operational Objective Analysis Schemes at the National Severe Storms Forecast Center. Rex L. Inman. November 1970. (COM-71-00136)
- No. 52 The Exploration of Certain Features of Tornado Dynamics Using a Laboratory Model. Neil B. Ward. November 1970. (COM-71-00139)
- No. 53 Rawinsonde Observation and Processing Techniques at the National Severe Storms Laboratory. Stanley L. Barnes, James H. Henderson and Robert J. Ketchum. April 1971.

No. 54 Model of Precipitation and Vertical Air Currents. Edwin Kessler and William C. Bumgarner. June 1971.

No. 55 The NSSL Surface Network and Observations of Hazardous Wind Gusts. Operations Staff. June 1971.

No. 56 Pilot Chaff Project at the National Severe Storms Laboratory. Edward A. Jessup. November 1971.